Materials Science and Engineering A 397 (2005) 239–248

MATERIALS SCIENCE & ENGINEERING A

www.elsevier.com/locate/msea

Factors affecting solidification thermal variables along the cross-section of horizontal cylindrical ingots

Eduardo Netto de Souza, Noé Cheung, Carlos Alexandre Santos, Amauri Garcia *

Department of Materials Engineering, State University of Campinas/UNICAMP, P.O. Box 6122, 13083-970 Campinas, SP, Brazil

Received 3 November 2004; received in revised form 8 February 2005; accepted 14 February 2005

Abstract

During solidification the mathematical analysis of heat flow depends on the transient heat transfer coefficient at the metal/mold interface. The analysis of heat transfer behavior along the cross-section of radial geometries is necessary for a better control of solidification in conventional foundry and continuous casting processes. For this purpose, a water-cooled solidification experimental apparatus was developed, and experiments were carried out with Sn–Pb alloys with different melt superheats. The transient metal/mold heat transfer coefficients were determined by a numerical-experimental fit of casting thermal profiles based on inverse heat transfer calculations. The results have shown a significant variation in heat flow conditions along the cylinder cross-section provoked by the simultaneous action of solidification thermal contraction and the gravitational effect. Experimental equations correlating heat transfer coefficients as a power function of time along the cross-section of cylindrical horizontal castings of Sn–Pb alloys are proposed.

Keywords: Solidification; Metal/mold heat transfer coefficient; Horizontal cylinders; Sn–Pb alloys

1. Introduction

The increased use of solidification modeling in the casting industry has reaped a number of benefits in terms of energy and scrap savings, in addition to improvements in product quality and consistency. The quality of castings can be greatly improved by exploiting the results of solidification modeling to predict macrostructural and microstructural features [1,2], to predict shrinkage and porosity defects [3,4], to predict mold filling [5], and to predict stress defects that form during solidification [6]. These models require reliable thermo-physical property data to obtain accurate predictions of the casting process. In particular, the thermal properties of materials used in the casting process must be known as well as the boundary conditions of the problem, usually expressed as cooling/mold and metal/mold heat-transfer coefficients or heat fluxes.

During solidification of a casting, the heat transfer between the casting surface and the mold is one of the most important factors that influence the solidification process, the resulting mechanical properties of the cast product and the cast product soundness [7,8]. It is primarily controlled by conditions at the metal–mold interface. There are several factors, which determine the thermal resistance and the heat flux at the metal/mold interface, such as the imperfectness of the thermal contact at this interface, nature and thickness of mold coating and the evolution of an air gap during solidification.

The metal's contraction phenomenon, the physical and chemical characteristics of both metal and mold, and the mold expansion during solidification, are mechanisms, which are responsible for the air gap formation at the metal/mold interface. In the beginning of the process, when the metal is completely liquid, the thermal contact is more effective due to the higher fluidity and metalostatic pressure effects. However, with the evolution of solidification, the thermal and volumetric contraction generated by the liquid/solid transformation creates a physical space at the interface, increasing in this way, the thermal resistance to the heat flowing into the

* Corresponding author. Tel.: +55 19 3788 3309; fax: +55 19 3289 3722.
E-mail address: amaurig@fem.unicamp.br (A. Garcia).

0921-5093/$ – see front matter © 2005 Elsevier B.V. All rights reserved.
doi:10.1016/j.msea.2005.02.044

mold. Thus, the thermal behavior of the interface varies with location from the interface and with time as solidification progresses. In addition, the orientation of the casting–mold interface with respect to gravity has a strong influence on the pressure between the casting and the mould surfaces at this interface. For horizontal cylinders, air gap width varies along the cross-section during solidification. The weight of the casting results in good thermal contact between the casting and the chill mold at the bottom. The angular contact gradually becomes poorer from the bottom ($\theta = 0^\circ$) to the side ($\theta = 90^\circ$) and top ($\theta = 180^\circ$) along the casting/mold interface.

The importance of determining this interface condition lies in the fact that it decisively influences cooling rate and solidification time in metallic molds. Numerous studies have been devoted to the measurement and determination of this boundary value [9–14].

Generally, two kinds of methods have been used in the determination of the transient metal/mold interfacial heat-transfer coefficient (h_i): (i) the air gap size is measured and this information associated with an integrated heat transfer and thermo-mechanical stress model which determines (h_i) [15]; (ii) inverse heat transfer calculations are performed based on temperature measurements at selected locations in the casting and the mould [16].

In cooled molds, the overall metal/mold heat transfer coefficient can be defined by a series of thermal resistances (R_T). The interfacial resistance between the casting and the mold inner surface ($R_{T_i} = 1/h_i$) is generally the largest, and the overall thermal resistance ($R_T = l/h$) is given by [17]:

$$\frac{1}{h} = \frac{1}{h_i} + \frac{e_s}{K_s} + \frac{e_c}{K_c} + \frac{1}{h_w} \quad (1)$$

where h is the overall heat transfer coefficient between the casting surface and the coolant fluid [W/m^2 K], h_i the heat transfer coefficient between metal and mold surfaces, e_c and e_s, are, respectively, the mold-coating thickness and the mold thickness (m), K_c and K_s are the coating and the mold thermal conductivities [W/m K], respectively, and h_w is the mold-coolant heat transfer coefficient.

Some experimental studies [18–20] have determined the transient heat transfer coefficient at the metal/mold interface (h_i) in cylindrical ingots, but they have not considered the angular variation of the gap along the cross-section. The present work is aimed to implement the approach of the inverse heat transfer calculation, to study the heat transfer during solidification of Sn–Pb alloys in a horizontal cylindrical chilled mold and to determine the time-dependent overall heat transfer coefficient considering the angular variation along the cylinder cross-section.

2. Experimental procedure

The experimental apparatus, schematically shown in Fig. 1, consists of a horizontal cylindrical chill made of stainless steel with heat insulating materials on the top to ensure

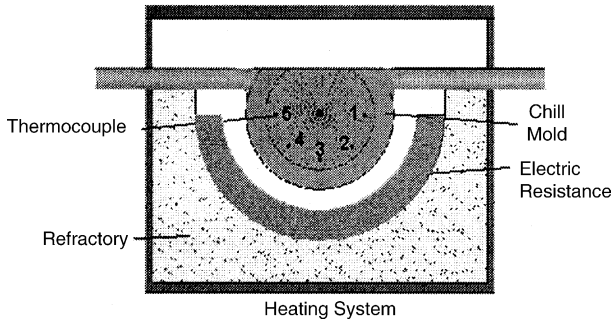

Fig. 1. Schematic representation of the experimental setup and thermocouple positions.

that a one-dimensional heat flux from the casting to the mold can be achieved along the radial direction. The inner surface of the mold is machine finished and no coatings had been applied. The alloys were melted in situ and the lateral electric heaters had their power controlled in order for a desired superheat (ΔT) to be achieved. When the desired melt temperature (melt superheat) is attained, the heating system is taken off and the mold is cooled by water. The cooling system was designed in such way that the water flow guarantees an extraction of heat essentially along the radial direction during solidification. The water flow was kept constant about 20 l/min, and controlled by a rotameter. In order to obtain the experimental temperature profiles, iron-constantan thermocouples were located in five positions along the cross-section, as shown in Fig. 1.

Fig. 2 shows a perspective view of the cooled chill mold used in the experiments, while Fig. 3 shows its cross-section with the respective dimensions. The thermocouples were fixed in a drilled support, with holes of 1.5 mm in diameter. The thermocouples were placed longitudinally along the casting at positions located 5 mm from the metal/mold interface,

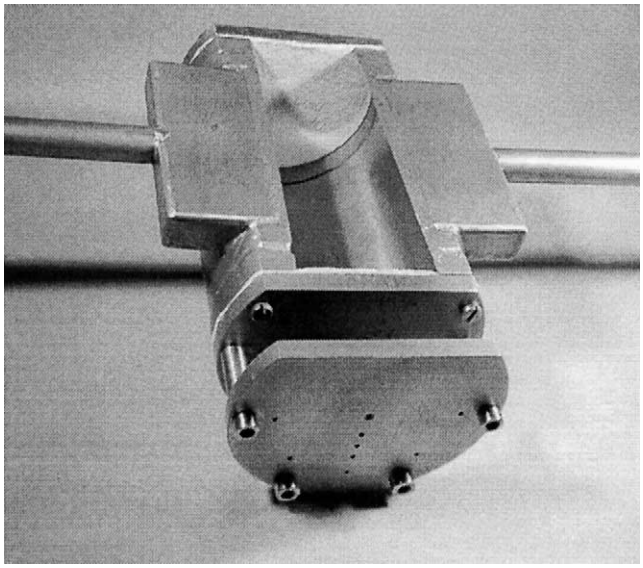

Fig. 2. Stainless steel chill mold.

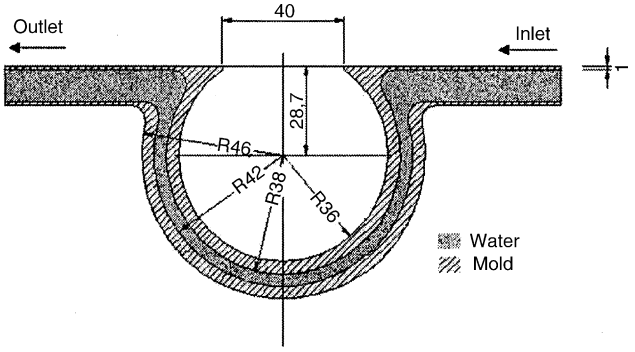

Fig. 3. Cross-section and dimensions of the chill mold (mm).

spaced in 45° angular increments, as shown. Temperature measurements were collected from each of the froe thermocouples at a frequency of 1 Hz. After solidification, the ingot is sectioned and examined to confirm the thermocouple positions.

Experiments were carried-out with Sn–5 wt.% Pb and Sn–15 wt.% Pb alloys with melt superheats, i.e., the initial melt temperature, of 3 and 20% above the liquidus temperature. The chemical compositions of commercially pure metals used to prepare these alloys are presented in Table 1. A solution containing 55 g of $FeCl_3$ and 4 ml HCl for each 150 ml of water was used to reveal the ingots macrostructures.

3. Numerical model

The mathematical model is based on the general equation of heat conduction [21] expressed in cylindrical coordinates:

$$\frac{1}{r}\frac{\partial}{\partial r}\left(Kr\frac{\partial T}{\partial r}\right)+\frac{1}{r^2}\frac{\partial}{\partial \phi}\left(K\frac{\partial T}{\partial \phi}\right)+\frac{\partial}{\partial z}\left(K\frac{\partial T}{\partial z}\right)+\dot{q}=\rho c\frac{\partial T}{\partial t} \quad (2)$$

where r, z and ϕ are the cylindrical coordinates represented in Fig. 4; ρ, c and K are, respectively, density (kg/m^3), specific heat (J/kg K) and thermal conductivity (W/m K).

The term of the heat generation of energy ($\dot{q}$) in the unsteady state condition is:

$$\dot{q}=\rho L\frac{\partial f_s}{\partial t} \quad (3)$$

where f_s is the solid fraction and L the latent heat of fusion (J/kg).

The fraction of solid in the mushy zone is estimated by Scheil equation, which assumes perfect mixing in the liquid and no solid diffusion. Assuming liquidus and solidus isotherms having constant slopes, f_s is then expressed by:

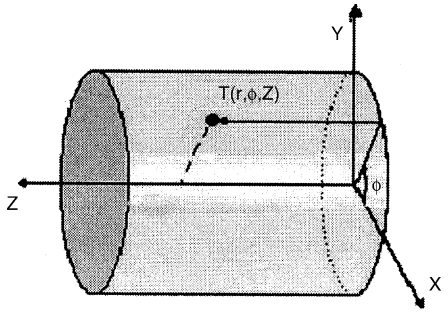

Fig. 4. Cylindrical coordinate system.

$$f_s=1-\left(\frac{T_f-T}{T_f-T_L}\right)^{1/k-1} \quad (4)$$

where T_f is the melting temperature (K), T_L the liquidus temperature and k the partition coefficient.

Eq. (4) is incorporated into the latent heat term (Eq. (3)) by differentiating Scheil's Equation with respect to temperature. Hence, applying the chain rule of differentiation, we have:

$$\frac{\partial f_s}{\partial t}=\frac{1}{(k-1)(T_f-T_L)}\left(\frac{T_f-T}{T_f-T_L}\right)^{(2-k)/(k-1)}\frac{\partial T}{\partial t} \quad (5)$$

The latent heat released during solidification of the remaining liquid of eutectic composition was taken into account by a device, which considers a temperature accumulation factor.

Considering that the flow of heat is mostly radial, Eq. (2) can be approximated by the one-dimensional form. Thus, the direction z of heat extraction can be neglected, since it is not significant compared to the heat flow in r and ϕ directions. For ingots with a symmetrical section, heat flow in the ϕ direction can also be neglected, resulting in a simplified equation:

$$\frac{1}{r}\frac{\partial}{\partial r}\left(Kr\frac{\partial T}{\partial r}\right)+\rho L\frac{\partial f_s}{\partial t}=\rho c\frac{\partial T}{\partial t} \quad (6)$$

Substituting Eq. (3) into Eq. (6) gives:

$$\frac{1}{r}\frac{\partial}{\partial r}\left(Kr\frac{\partial T}{\partial r}\right)=\rho c'\frac{\partial T}{\partial t} \quad (7)$$

where

$$c'=\left(c-L\frac{\partial f_s}{\partial T}\right) \quad (8)$$

The term c', known as the effective specific heat, accounts for both temperature change as well as the latent heat liberation associated with the phase transformation in the temperature range (T_S, T_L).

Table 1
Chemical analyses of metals used to prepare Sn–Pb alloys

Metal	Fe	Ni	Cu	Pb	Mn	Zn	Sn
Chemical composition (wt.%)							
Sn	0.009	–	0.007	0.19	0.0025	–	
Pb	0.002	0.003	–		–	0.003	0.25

At the range of temperatures where solidification occurs for metallic alloys, the physical properties will be evaluated, taking into account the amount of liquid and solid that coexists in equilibrium at each temperature:

$$c = (1 - f_s)c_L + f_s c_s \tag{9}$$

$$K = (1 - f_s)K_L + f_s K_s \tag{10}$$

$$\rho = (1 - f_s)\rho_L + f_s \rho_s \tag{11}$$

A finite difference form of Eq. (7) is obtained for the time-dependent temperature distribution at discrete grid points:

$$T_i^{n+1} = \frac{\Delta t}{\rho_i c_i' r_i \Delta r^2}[K_{\text{eq}\,i-1} r_{i-1}(T_{i-1}^n - T_i^n) + K_{\text{eq}\,i+1} r_{i+1}(T_{i+1}^n - T_i^n)] + T_i^n \quad \text{for } i \neq 0 \tag{12}$$

where the subscript i represents the location of the element in the finite difference mesh, and $(n+1)$ represents the instant in which the nodal temperature is being calculated, as represented in the nodal network shown in Fig. 5. The K_{eq} is the equivalent thermal conductivity in terms of the thermal conductivity of an adjacent element and itself, given by [1]:

$$K_{\text{eq}\,i+1} = \frac{2K_{i+1}K_i}{K_{i+1} + K_i} \tag{13}$$

$$K_{\text{eq}\,i-1} = \frac{2K_{i-1}K_i}{K_{i-1} + K_i} \tag{14}$$

3.1. Boundary conditions

3.1.1. Center of the casting

When the limit of (r) tends to zero, there is an indetermination in the left side of Eq. (7). L'Hopital rule has been used to solve this indetermination and states that differentiation of both the numerator and denominator does not change the limit. This differentiation often simplifies the quotient and/or converts it to a determinate form, allowing the limit to be determined more easily. Applying L'Hopital rule and the finite difference method in Eq. (7), we obtain for $i = 0$:

$$T_0^{n+1} = 4 \cdot \frac{K_{eq1} \cdot \Delta t}{\rho_0 \cdot c_0} \cdot \left(\frac{T_1^n - T_0^n}{\Delta r^2}\right) + T_0^n \tag{15}$$

3.1.2. Metal

Inside the metal, the following equation is applied:

$$T_i^{n+1} = \frac{\Delta t}{\rho_i c_i' r_i \Delta r^2}[K_{\text{eq}\,i-1} r_{i-(1/2)}(T_{i-1}^n - T_i^n) + K_{\text{eq}\,i+1} r_{i+(1/2)}(T_{i+1}^n - T_i^n)] + T_i^n \tag{16}$$

3.1.3. Metal/coolant interface

Considering the metal/coolant heat transfer, the following equation can be obtained by applying a thermal balance:

$$T_m^{n+1} = \frac{\Delta t}{\rho \cdot c' \cdot r_m \cdot \Delta r}\left[h \cdot r \cdot (T_a^n - T_m^n) + K_{\text{eq}\,m-1} \cdot r_{m-1} \cdot \frac{T_{m-1}^n - T_m^n}{\Delta r}\right] + T_m^n \tag{17}$$

where r_m is external radius of the cylindrical ingot, T_a^n the environment temperature, m the location of the element in finite difference mesh regarding to the external radius of the cylindrical ingot and h is the overall heat transfer coefficient between the casting surface and the coolant fluid. As mold coatings are not being used, Eq. (1) is given by:

$$\frac{1}{h} = \frac{1}{h_i} + \frac{e_s}{K_s} + \frac{1}{h_w} \tag{18}$$

The method used to determine the transient metal/coolant heat transfer coefficient, h, is based on the solution of the inverse heat conduction problem (IHCP) [16]. This method makes a complete mathematical description of the physics of the process and is supported by temperature measurements at known locations inside the heat conducting body. The temperature files containing the experimentally monitored temperatures are used in a finite difference heat flow model to determine h. The process at each time step included the following: a suitable initial value of h is assumed and with this value, the temperature of each reference location in casting at the end of each time interval Δt is simulated by the numerical model. The correction in h at each interaction step is made by a value Δh, and new temperatures are estimated $[T_{est}(h + \Delta h)]$ or $[T_{est}(h - \Delta h)]$. With these values, sensitivity

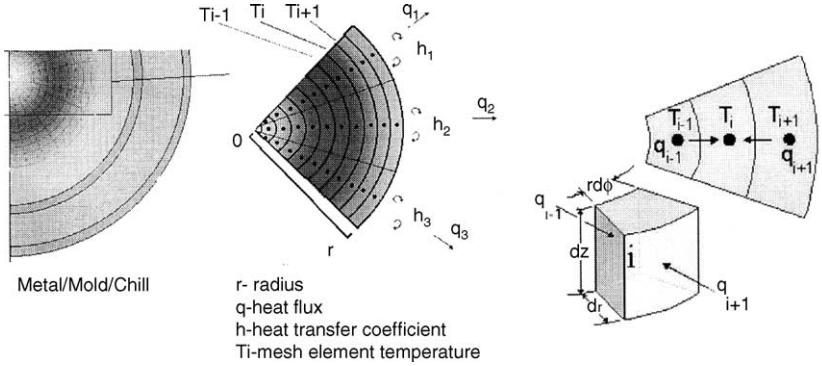

Fig. 5. FDM mesh applied at the cross-section of the metal/mold cylindrical system.

Table 2
Thermophysical properties [22–27]

	Sn–5 wt.% Pb	Sn–15 wt.% Pb	Sn–20 wt.% Pb	Eutectic
K_s (W/mK)	65.4	62.2	60.5	54.4
K_L (W/mK)	32.8	32.5	32.3	31.7
ρ_s (kg/m^3)	7184	7906	8108	8875
ρ_L (kg/m^3)	7184	7551.7	7735.6	8434
c_s (J/kg K)	216.4	207.3	202.8	185.4
c_L (J/kg K)	253	240.9	234.8	211.9
L (J/kg)	58985	55534	53809	47253
T_L (K)	225	210	203	–
T_E (K)	183	183	183	183
T_F (K)	232	232	232	–
k	0.0656	0.0656	0.0656	0.0656

coefficients (ϕ) are calculated for each interaction, given by:

$$\phi = \frac{T_{est}(h + \Delta h) - T_{est}(h)}{\Delta h_i} \quad (19)$$

The procedure determines the value of h, which minimizes an objective function defined by:

$$F(h) = \sum_{i=1}^{n} (T_{est} - T_{exp})^2 \quad (20)$$

where T_{est} and T_{exp} are the estimated and the experimentally measured temperatures at various thermocouples locations and times, and n the iteration stage. The applied method is a simulation assisted one and has been used in recent publications for determining h for a number of solidification situations [10,14] based on fitted calculations of the heat transfer coefficients.

The thermophysical properties of the alloys used presently in the simulations performed with the developed solidification model are shown in Table 2.

4. Results and discussion

The temperature measurements have shown that the experimental apparatus permitted an essentially constant melt temperature to be attained before the beginning of cooling, avoiding, hence, significant thermal gradients inside the liquid metal. The columnar structures in the longitudinal and radial directions reveal an essential one-dimensional radial heat flow situation, as shown in Fig. 6. The end of the solidification occurs above the geometric center of the casting, indicating variation of heat flow at the metal/mold interface along the cylinder cross-section. The structure indicates that the heat transfer was more effective at the bottom, decreasing along the cylinder surface toward the top.

The effect of the air gap evolution is better visualized throughout the experimental temperature cooling curves monitored in different points inside the casting located at 5 mm from the metal/mold interface. Figs. 7 and 8 show the comparison between experimental thermal responses and those which resulted from individual simulations for the Sn–5 wt.% Pb and Sn–15 wt.% Pb alloy castings, with an initial melt temperature of about 20 and 3% above the liquidus temperature, respectively. Positions 4 and 5 were not used in the numerical simulations because their thermal responses were equal to the symmetric positions, i.e., positions 2 and 1, respectively (Fig. 9).

In order to parameterize h with time, the software Microcal Origin was used which is based on the Classical Freundlinch Model of least square minimization. The results of thermal analysis show a decrease on the thermal contact between the metal and the mold, with the angular variation toward the casting top. The metal contraction at the bottom zone of the ingot is less pronounced than at the other regions due to the gravitational effect. Tables 3 and 4 show the resulting equation describing the metal/mold transient heat transfer coefficients (h), at characteristic positions along the cylinder cross-section. They express h as a power function of time,

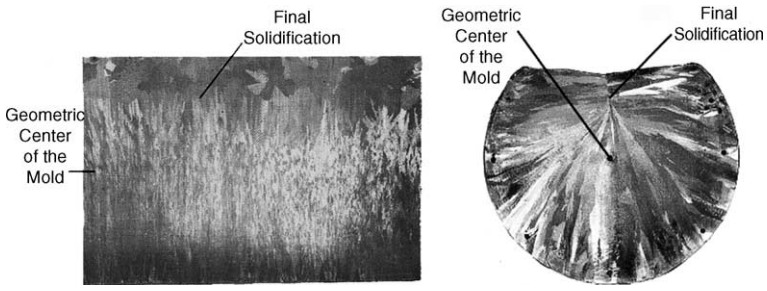

Fig. 6. Typical macrostructure (longitudinal and transversal) of the cylindrical casting cross-section: Sn–5 wt.% Pb, initial melt temperature (T_p) = 252 °C. Magnification: 1×.

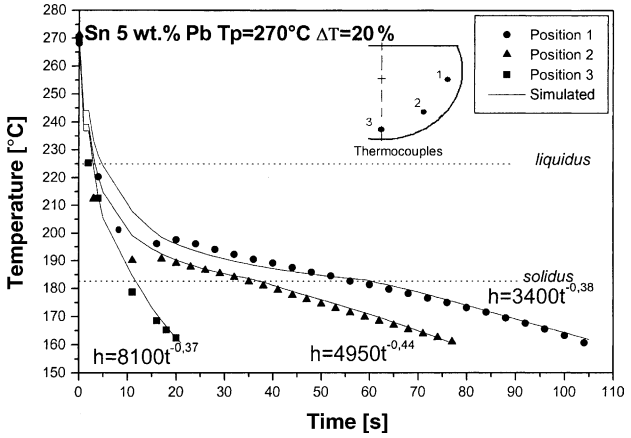

Fig. 7. Experimental and simulated temperatures: Sn–5 wt.% Pb; $T_P = 270\,^{\circ}C$.

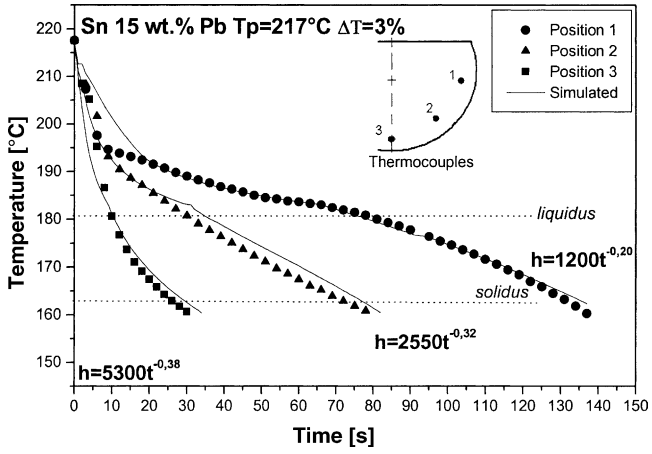

Fig. 8. Experimental and simulated temperatures: Sn–15 wt.% Pb; $T_P = 217\,^{\circ}C$.

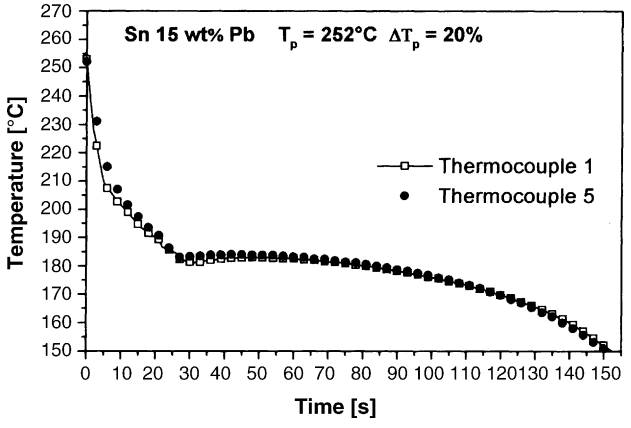

Fig. 9. Comparison between thermocouples 1 and 5 (Sn–15 wt.% Pb).

given by:

$$h = at^{-m} \tag{21}$$

where t is the time (s), m and a are constants which depend on alloy composition and solidification conditions.

Table 3
Transient heat transfer coefficients for Sn–5 wt.% Pb cylindrical castings

Position	Sn–5 wt.% Pb	
	$T_p = 232\,^{\circ}C$	$T_p = 270\,^{\circ}C$
1 (lateral)	$h = 2150t^{-0.27}$	$h = 3400t^{-0.38}$
2 (45°)	$h = 3950t^{-0.33}$	$h = 4950t^{-0.44}$
3 (bottom)	$h = 4500t^{-0.25}$	$h = 8100t^{-0.37}$

Table 4
Transient heat transfer coefficients for Sn–15 wt.% Pb cylindrical castings

Position	Sn–15 wt.% Pb	
	$T_p = 217\,^{\circ}C$	$T_p = 252\,^{\circ}C$
1 (lateral)	$h = 1200t^{-0.20}$	$h = 1800t^{-0.35}$
2 (45°)	$h = 2550t^{-0.32}$	$h = 2650t^{-0.32}$
3 (bottom)	$h = 5300t^{-0.38}$	$h = 4500t^{-0.26}$

The metal/mold transient heat transfer coefficients (h) expressed as a power function of time can be taken as a general trend, but care should be exercised when applying the expression to the beginning of solidification. A more complex experimental set-up with a higher frequency of temperature acquisition would be necessary for accurate characterization of initial values of heat transfer coefficients (e.g. time <3 s) for the present experiment. The variation of metal/coolant heat transfer coefficient, h, as a function of time, is shown in Figs. 10–13. The h curves show that for all positions (1–3) the heat transfer coefficient profiles drop rapidly as a result of gap formation at the initial stage of solidification, but then the h value reaches approximately a steady value. It can be seen that a significant difference in metal/mold heat transfer efficiency exists along the cross-section of horizontal cylindrical castings. The difference is greater between positions 1 and 3, due to the progressive decrease of the gravitational influence. It can be seen that higher h profiles are obtained as the melt superheat is increased. Campbell reports that the fluidity of molten Sn–Pb alloys increase with increasing superheat, favoring the wetting of the chill by the melt [28]. This fact is

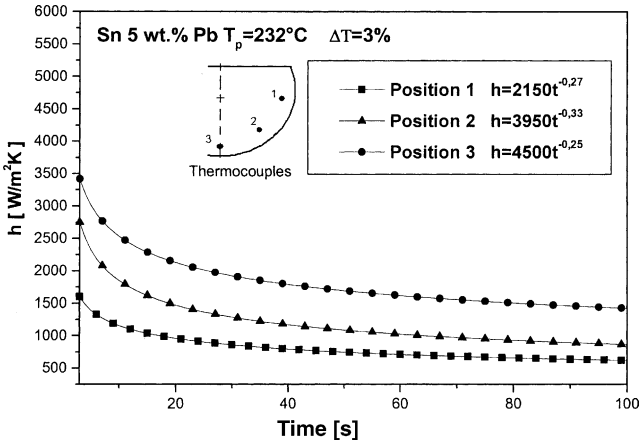

Fig. 10. Metal/coolant heat transfer coefficient as a function of time: Sn–5 wt.% Pb; $T_P = 232\,^{\circ}C$.

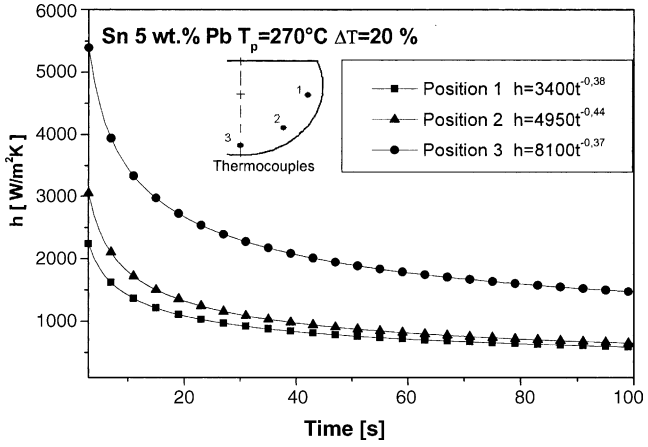

Fig. 11. Metal/coolant heat transfer coefficient as a function of time: Sn–5 wt.% Pb; $T_P = 270\,^{\circ}C$.

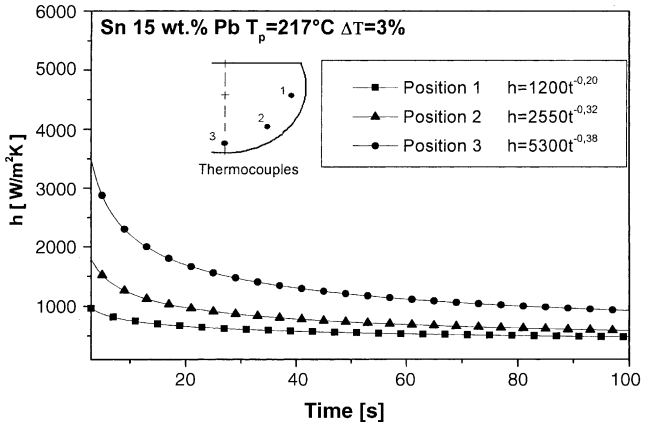

Fig. 12. Metal/coolant heat transfer coefficient as a function of time: Sn–15 wt.% Pb; $T_P = 217\,^{\circ}C$.

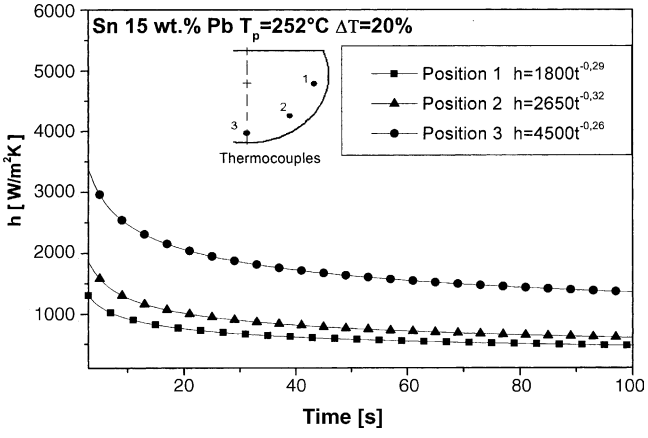

Fig. 13. Metal/coolant heat transfer coefficient as a function of time: Sn–15 wt.% Pb; $T_P = 252\,^{\circ}C$.

more evident in the Sn–5 wt.% Pb than in the Sn–15 wt.% Pb alloy.

The influence of alloy composition on heat transfer coefficient is shown in Fig. 14 for the bottom position (position 3). It can be seen that the h profiles for Sn–20 wt.% Pb and

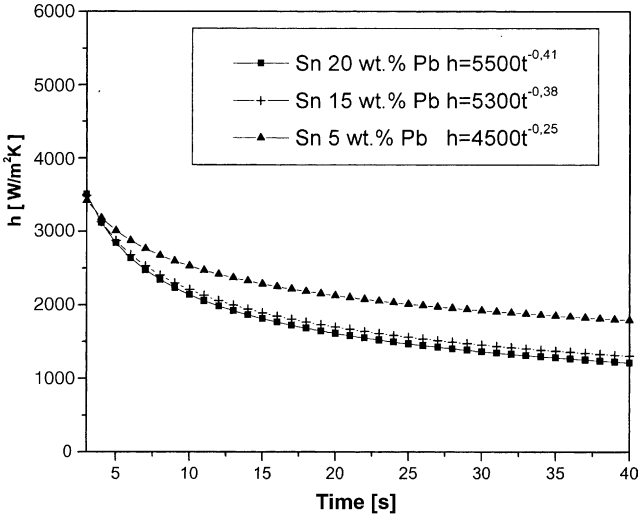

Fig. 14. Metal/coolant heat transfer coefficient as a function of time for different alloy compositions: bottom part of the mold (position 3). Melt superheat: 3% above liquidus temperature.

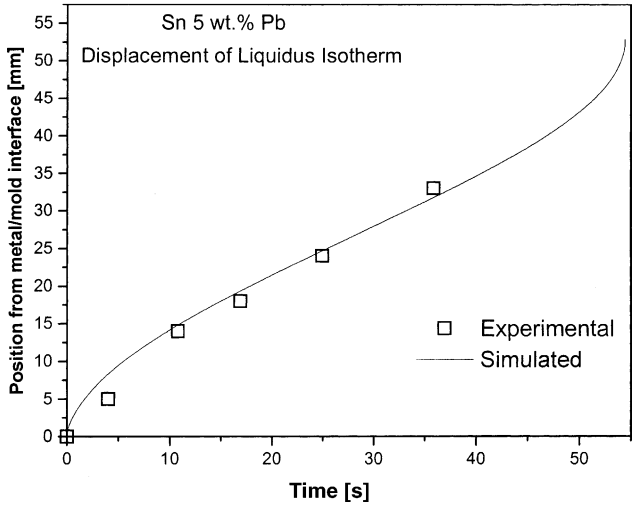

Fig. 15. Position of liquidus isotherm as a function of time: Sn–5 wt.% Pb; $h = 4500t^{-0.25}$; $T_P = 232\,^{\circ}C$.

the Sn–15 wt.% Pb alloy castings are similar. Experiments performed in a vertical upward solidification mold, also using Sn–Pb alloys [2], show the same behavior of h profiles according to the alloy composition, i.e., lower h profiles are obtained as the solute concentration is increased.

The results of thermal analysis in metal have also been used to determine the displacement of the liquidus isotherm as a function of time. The thermocouples readings have been used to generate a plot of position from the metal/mold interface as a function of time corresponding to the liquidus front passing by each thermocouple. A curve fitting technique on these experimental points has generated a power function of position as a function of time. The derivative of this function with respect to time has yielded values for tip growth rate. Figs. 15–17 show experimental positions of liquidus isotherm, at the bottom zone of the ingot, compared with

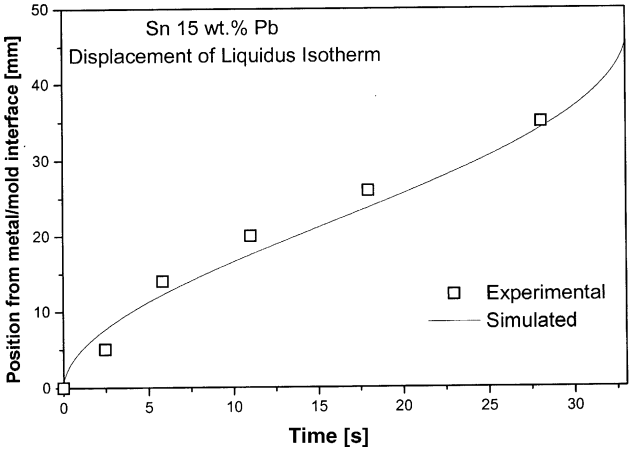

Fig. 16. Position of liquidus isotherm as a function of time: Sn–15 wt.% Pb; $h = 5300t^{-0.38}$; $T_P = 217\,^{\circ}C$.

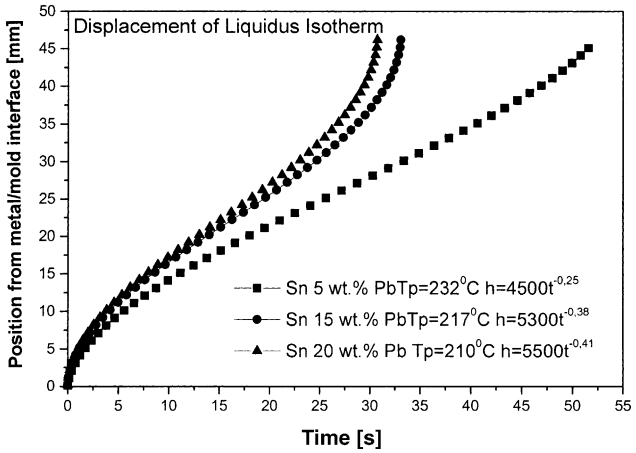

Fig. 18. Comparative displacement of liquidus isotherm.

theoretical results furnished by the numerical solidification model, which used the corresponding transient heat-transfer coefficient profile. A marked increase on tip growth rate near the end of the casting, given by the slope of these curves, can be observed. One can realize a good agreement between the experimental values and those numerically simulated. Fig. 18 shows a comparison of liquidus isotherm displacement for the three alloys experimentally examined. A progressive increase in tip growth rate with increasing solute content can be observed.

The influence of melt superheat on the displacement of liquidus isotherm during solidification is analyzed in Fig. 19 for a Sn–15 wt.% Pb alloy, solidified under two conditions of initial melt temperature: 3 and 20% above the liquidus temperature, and considering heat flow conditions at the casting bottom.

It can be seen that, the higher melt superheat induces a slower displacement of the liquidus isotherm despite the slightly higher h profile is observed as the superheat increases. During solidification, varying tip growth rate and temperature gradients can lead to different structural morphologies, including planar, cellular, columnar dendritic or equiaxed dendritic microstructures [17,27]. The time dependent boundary (h) is one of the main factors affecting these solidification variables. Fig. 20 shows the evolution of tip growth rate as a function of position from cylinder surface, and considering heat flow conditions at the casting bottom (Sn–5 wt.% Pb alloy with 3% of melt superheat). It can be seen that the tip growth rate is high at the beginning of solidification and decreases up to the point where geometrical effects [29,30] induce an increase in growth rate. The solidification of round sections has particular characteristics, which diverge from the behavior observed in the solidification of billets and slabs, where the surface of the moving solid/liquid front is equivalent to the heat exchange surface at the casting/mold interface. In spherical and cylindrical inward solidification, the flow of heat is purely radial and the solid/liquid surface decreases gradually as the freezing front approaches the center of the body. As a direct consequence, the volume of liquid during solidification will also decrease, being reduced to a point (spheres) and a line (cylinders) at

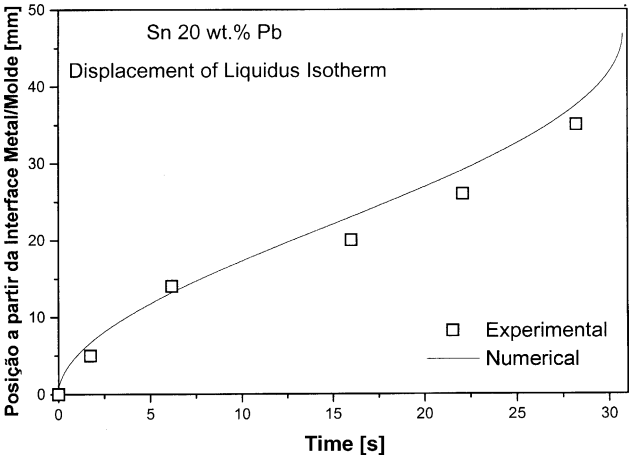

Fig. 17. Position of liquidus isotherm as a function of time: Sn–20 wt.% Pb; $h = 5500t^{-0.41}$; $T_P = 210\,^{\circ}C$.

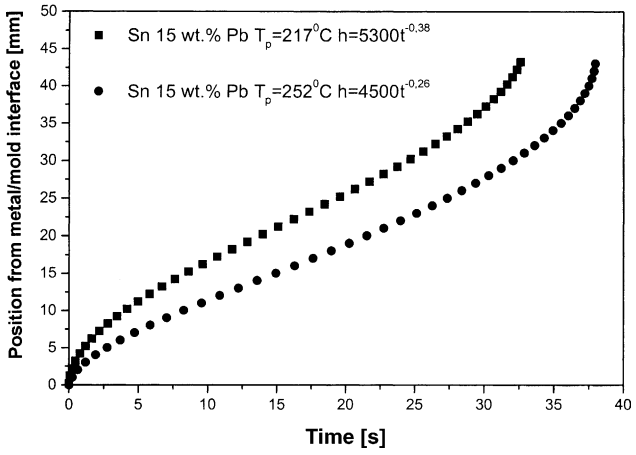

Fig. 19. Influence of melt superheat on the displacement of liquidus isotherm.

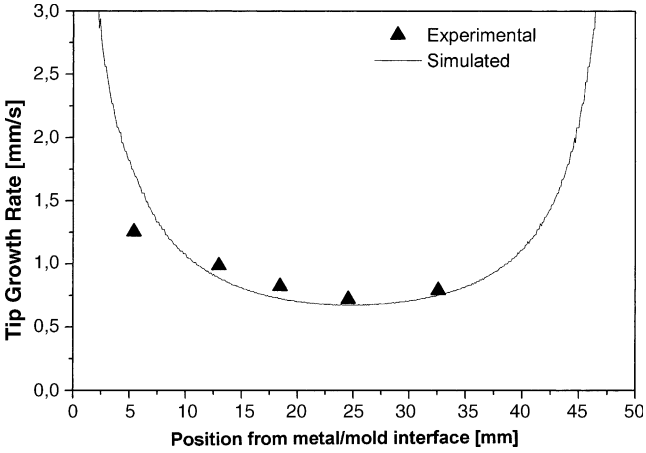

Fig. 20. Tip growth rate as function of position from cylinder surface: Sn–5 wt.% Pb.

the end of solidification. Under these circumstances it is not difficult to visualize that the growth rate will be high at the casting surface and will decrease gradually with the growing solidified shell up to a point where the remaining volume of liquid equals the volume of solidified material. It will then increase again tending to an infinite theoretical value at the cylinder/sphere center. This behavior will have as a determinant characteristic, a point where the tendency of growth rate is reverted (reversion point), which will depend on the radial geometry, interfacial heat transfer coefficient and on the thermophysical properties of metal and mold. In Fig. 21 the inverse of tip growth rate is plotted against the distance from metal/mold interface in order to determine the location where growth rate reversion occurs. Applying their analytical model for inward solidification of cylinders, and spheres, Santos and Garcia [31] have determined that this reversion point lies between 0.4 and 0.5 of the radius for the cylindrical solidification, and are dependent of both Stefan and Biot numbers. Fig. 21 shows that the reversion point for the present investigation has occurred about half of the cylinder radius.

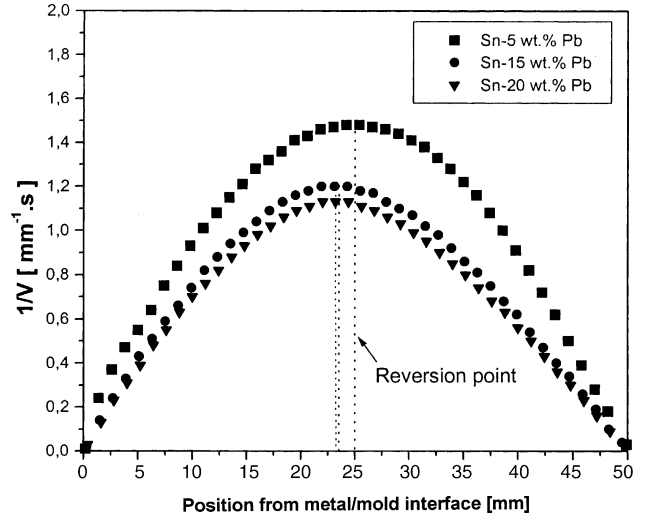

Fig. 21. Comparison of position of growth rate reversion. Melt superheat: 3%; bottom (position 3).

5. Conclusions

Experiments were conducted to analyze the behavior of metal–mold heat transfer coefficients (h) and tip growth rate during solidification of Sn–Pb alloys in a horizontal cylindrical stainless steel water-cooled chill. The following conclusions can be drawn:

- A significant difference in metal/mold heat transfer coefficient, h, exists around the circumference of the casting due to differences on the air gap width. From the bottom to the side, the maximum value of h drops about 48% and 23% for Sn–5 wt.% Pb and Sn–15 wt.% Pb alloys, respectively, for a melt superheat of 3% above the liquidus temperature.
- Higher h profiles were obtained as the melt superheat was increased.
- Lower h profiles were observed as the alloy solute content was increased.
- A good agreement has been observed between the experimental values of tip growth rate and those numerically simulated. A progressive increase in tip growth rate with increasing alloy solute content has been detected.
- The tip growth rate is high at the beginning of solidification and decreases up to a point where geometrical effects induce an increase in growth rate toward the cylinder center. This reversion point, determined by the used numerical/experimental approach, is located at a distance of about 0.5 of the cylinder radius, which is inside the range suggested by earlier theoretical predictions.

Acknowledgements

The authors acknowledge financial support provided by FAPESP (The Scientific Research Foundation of the State of São Paulo, Brazil), and CNPq (The Brazilian Research Council).

References

[1] O.F.L. Rocha, C.A. Siqueira, A. Garcia, Mater. Sci. Eng. A 347 (2003) 59–69.
[2] O.F.L. Rocha, C.A. Siqueira, A. Garcia, Metall. Mater. Trans. A 34 (2003) 995–1006.
[3] S. Bounds, G. Mora, K. Pericleous, M. Cross, T.N. Croft, Metall. Mater. Trans. B 31 (2000) 515–527.
[4] A.S. Sabau, S. Viswanathan, Metall. Mater. Trans. B 33 (2002) 243–255.
[5] G.B. Van Der Graaf, H.E.A. Van Den Akker, L. Katgerman, Metall. Mater. Trans. B 32 (2001) 69–78.
[6] A.K. Dahle, S. Instone, T. Sumitomo, Metall. Mater. Trans. A 34 (2003) 105–113.

[7] W.R.R. Osório, C.A. Santos, J.M.V. Quaresma, A. Garcia, J. Mater. Proc. Technol. 143/44 (2003) 703–709.
[8] J.M.V. Quaresma, C.A. Santos, A. Garcia, Metall. Mater. Trans. A 31 (2000) 3167–3177.
[9] N.J. Goudie, S.A. Argyropoulos, Can. Metall. Quart. 34 (1995) 73–84.
[10] M. Krishnan, D.G.R. Sharma, Int. Comm. Heat Mass Transfer 23 (1996) 203–214.
[11] J.H. Lee, H.S. Kim, C.W. Won, B. Cantor, Mater. Sci. Eng. A 328 (2002) 182–190.
[12] T. Loulou, E.A. Artyukhin, J.P. Bardon, Int. J. Heat Mass Transfer 42 (1999) 2119–2127.
[13] M.A. Martorano, J.D.T. Capocchi, Int. J. Heat Mass Transfer 43 (2000) 2541–2552.
[14] C.A. Santos, J.M.V. Quaresma, A. Garcia, J. Alloys Comp. 319 (2001) 174–186.
[15] M. Trovant, S.A. Argyropoulos, Can. Metall. Quart. 37 (1998) 185–196.
[16] J.V. Beck, Int. J. Heat Mass Transfer 13 (1970) 703–716.
[17] C.A. Siqueira, N. Cheung, A. Garcia, J. Alloys Comp. 351 (2003) 126–134.
[18] G. Fortin, P.R. Louchez, F.H. Samuel, La Revue of Métallurgie – CIT/Science et Génie des Matériaux (1994) 772–780.
[19] M. Trovant, S. Argylopoulos, Metall. Mater. Trans. B 31 (2000) 75–86.
[20] T.G. Kim, Z.H. Lee, Int. J. Heat Mass Transfer 40 (1997) 3513–3525.
[21] F.P. Incropera, D.P. Dewitt, Fundamentals of Heat and Mass Transfer, 3rd ed., John Wiley & Sons, New York, 1990.
[22] L.F. Mondolfo, Mater. Sci. Technol. 5 (1976) 118.
[23] R.D. Pehlke, Summary of Thermophysical Properties for Casting Alloys and Mold Materials, University of Michigan, 1982.
[24] Y.S. Toloukian, et al., Thermophysical Properties of Matter, vol. 1, IFI/Plenum, New York, 1970.
[25] A. Bejan, Heat Transfer, John Wiley & Sons, New York, 1993.
[26] D. Bouchard, J.S. Kirkaldy, Metall. Mater. Trans. B 28 (1997) 651–663.
[27] O.L. Rocha, C.A. Siqueira, A. Garcia, Mater. Sci. Eng. A 361 (2003) 111–118.
[28] J. Campbell, Castings, Butherworth Heinemann, London, 1991.
[29] D. Bouchard, J.S. Kirkaldy, Metall. Mater. Trans. B 27 (1996) 101–113.
[30] T.W. Clyne, Metall. Mater. Trans. B 13B (1982) 471–478.
[31] R.G. Santos, A. Garcia, Int. J. Cast. Res. 11 (1998) 187–195.